Extreme enhancement of the quality (Q)-factor and mode field intensity in cavity-resonator gratings

EVGENY POPOV,[1,*] ELIZABETH HEMSLEY,[1,2] ANNE-LAURE FEHREMBACH,[1] OLIVIER GAUTHIER-LAFAYE,[2] ANTOINE MONMAYRANT,[2] AND STÉPHANE CALVEZ[2]

[1]*Aix Marseille Univ, CNRS, Centrale Marseille, Institut Fresnel, Marseille, France*
[2]*LAAS-CNRS, Université de Toulouse, CNRS, 7 avenue du colonel Roche, F-31400 Toulouse, France*
*e.popov@fresnel.fr

Abstract: In this paper, dielectric Cavity-Resonant Integrated-Grating Filters (CRIGFs) are numerically optimized to achieve extremely high-quality factors, by optimizing the cavity in/out-coupling rate and by introducing apodizing mode-matching sections to reduce scattering losses. Q-factors ranging between 0.1 and 50 million are obtained and two different domains are distinguished, as a function of the perturbation parameter which controls the cavity in/out-coupling rate. When the cavity coupling Q-factor is lower than the Q-factor of the uncoupled Fabry-Perot cavity, corresponding to the over-coupling regime, the reflectivity response exhibits a high resonance maximum. On the contrary, in the under-coupling regime the resonant reflectivity maximum is much weaker since the scattering losses of the uncoupled cavity dominate. Between these two domains, the so-called critical coupling condition leads to very strong field enhancement inside the device, reaching up to 10^4 times the incident field amplitude. This theoretical work paves the way towards the practical implementation of CRIGFs with much higher Q-factors than currently demonstrated, potentially reaching performance on a par with other resonators such as photonic crystal cavities or whispering gallery mode resonators. These results can serve to optimize the design of narrow-band planar grating filters, particularly for application in non-linear optics.

1. Introduction

The use of zero-order dielectric gratings for spectral filtering started in 1978 with the work of Knop [1] on a large-band filter for color imaging. Several years later, narrow-band filtering was demonstrated [2], based on the Fano-type anomaly [3,4], the latter being caused by the excitation of waveguide modes in corrugated waveguides. The main advantage came from the fact that, irrespective of the grating parameters, when its groove profile is symmetric, the reflection maximum is theoretically guaranteed to reach 100% [5]. Consequently, any (large or small) spectral width of the anomaly can be obtained with a proper choice of the grating modulation strength. Theoretically, under plane-wave incident illumination, the angular tolerance imposed on the incident beam is determined mainly by the grating equation; the smaller the spectral width, the smaller the divergence of the beam required [6]. If this requirement were to be neglected, the theoretical 100% reflection maximum reduces and the spectral width increases. For example, a Q-factor of 10^6 requires width of the incident beam to be in excess of 5000 resonant wavelengths [7], requiring large and homogeneous beams and gratings.

It was necessary to wait until the new millennium in order to overcome this trade-off by placing the corrugated waveguide inside a resonator [8,9]. Indeed, in that case, the size of the cavity determines the working wavelength and significantly increases the angular tolerance. When planar Distributed Bragg Reflectors (DBR) form the external cavity, the device is known

under the name of cavity-resonator integrated grating filter (CRIGF). Applications have been demonstrated including narrow-band filtering of focused beams [10,11] using Si_3N_4/SiO_2 or GeO_2/SiO_2 materials, wavelength-stabilized external-cavity diode lasers [12,13] down to the mid-infrared using GaAs/AlGaAs materials, or second harmonic generation (SHG) [14–16] using lithium-on-insulator (LNOI) substrates. Nevertheless, to-date, the experimentally demonstrated CRIGFs exhibit Q-factors reaching, at the most, a few thousands [17], and CRIGF optimization remains limited to basic design considerations independent of the final applicative purpose.

In this paper, we propose new practical designs that alleviate these limitations and enable creation of CRIGFs with an extremely narrow-band spectral response ($Q > 10^7$) as calculated by the Fourier modal method (FMM) [18,19]. The main optimization principle consists of adjusting the grating coupling efficiency such that the waveguide cavity excitation meets the critical coupling condition, as defined for other resonators [20]. For high Q-factors, the predominant loss mechanism is due to transition scatter (originating from the difference in effective index between the central grating coupler (GC) and the surrounding cavity-building Distributed Bragg Reflectors (DBRs) – see Fig. 1). Therefore, an additional strategy is introduced to reduce these losses by insertion of apodizing regions at these junctions. Both improvements are successfully underpinned by the choice of bi-atom grating structures [21] with a shallow-depth profile modulation throughout the device. Finally, our analysis in terms of critical coupling allows us to develop design strategies adapted to promote narrow-band high reflectivity for filtering applications or high internal field for non-linear applications.
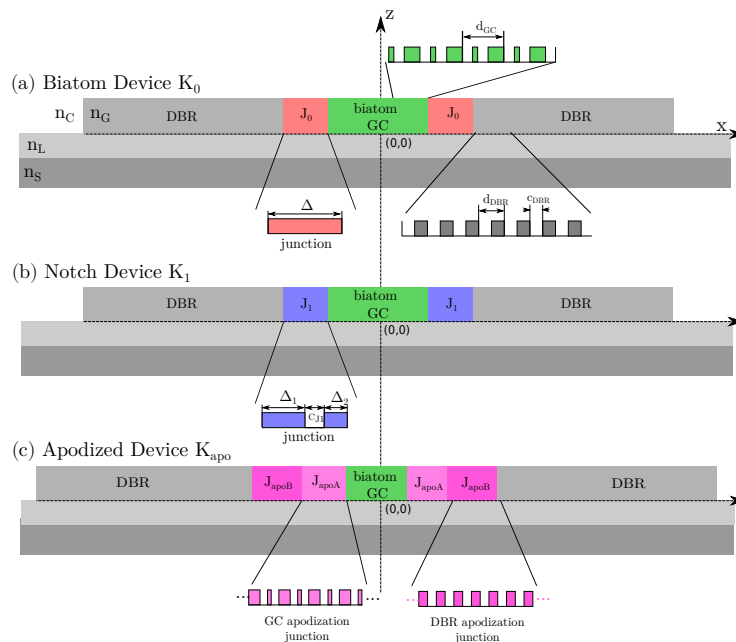
**Fig. 1.** Schematic presentation of the different CRIGF configurations.

2. CRIGF design

The CRIGF devices are presented schematically in Fig. 1. The typical device consists of a high-index waveguiding layer on a substrate covered with a lamellar grating. The latter serves as

a grating coupler between the waveguide mode and the incident Gaussian beam, impinging on the device at normal incidence. The GC is placed in a resonator cavity made of two Distributed Bragg Reflectors (DBR)s. The length of the junctions between the GC and the DBRs are chosen to tune the resonant wavelength to the chosen design value, 1.55 μm in our case. The pattern is considered infinite in y-direction. While the real structures have limited width, we have already shown in [19] that this has no impact on the CRIGF scattering properties, provided that the width is larger than twice its length. This study was made for smaller Q-factor (around 700), and should be extended for structures with greater Q-factors, but this is out the scope of this paper.

The values of the Q-factor for CRIGF devices known in the literature hardly exceed 20 000, although much higher values (up to 2×10^6) have been predicted by using the excitation of the antisymmetric (so called dark) modes of the device [16]. Further increase can be made by decreasing the grating efficiency of the GC, for example, by decreasing its groove depth. However, the depth of the DBR region must stay sufficiently high to ensure high reflectivity at a reasonable length. Using different groove depths for the different gratings of the device could be considered, but this approach requires challenging multi-etching fabrication processes with nanometric realignment. Additionally, such a choice also increases the difference between the modal field profiles between the GC and DBR regions and thus increases the losses due to the transitional scatter (S_{tr}) at these junctions. As shown further, these losses can become critical for large values of the Q-factor.

Keeping the groove depth of the GC region fixed leaves several options to reduce the modal excitation efficiency: 1) using a filling factor of the grooves considerably different from 0.5, although this implies that either the groove troughs or bumps have to be very narrow (tending to zero as the device Q-factor increases), creating technological difficulties; 2) exciting the "dark" mode, as we proposed in [16]; or 3) as explored in the present study, constructing a so-called bi-atom grating, consisting of double-feature grooves of overall period $2d_{DBR}$ (d_{DBR} being the period in the DBR regions) with different width a_1 and a_2 of the consecutive bumps and trough width $c_{GC}/2$ (see Fig. 2). While the filling factor can stay close to 0.5, the difference $\delta = (a_1 - a_2)/4$ serves as a small perturbation influencing the coupling in & out of the FP cavity. This approach allows to minimize the difference between the GC and DBR patterns, reducing the scatter losses at the junctions due to impedance mismatch.
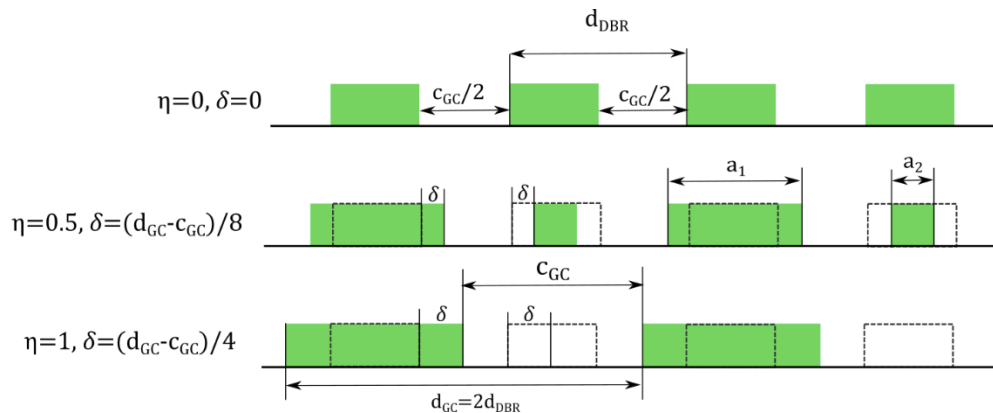
Fig. 2. Detailed view of the double-feature (bi-atom) structure of the GC, with perturbation parameter δ, and dimensionless parameter η.

Alternatively to the parameter δ, in order to be consistent with the literature on resonators, we will use in section 3 the dimensionless parameter:

$$\eta = \frac{\delta}{\delta_{max}} \qquad (1)$$

with $\delta_{max} = (d_{GC}-c_{GC})/4$ for which $a_2 = 0$ and a_1 is maximum (see Fig. 2). When $\eta = 0$ ($\delta = 0$ nm), the profile corresponds to a DBR with a fill factor $c_{GC}/(2d_{DBR})$, and there is no coupling between the cavity and the free-space incoming beam. When $\eta = 1$ ($\delta = \delta_{max}$), the profile corresponds to a standard GC with a fill factor $c_{GC}/d_{GC} = c_{GC}/(2d_{DBR})$, and the in/out-coupling is maximum.

Hereafter, we consider a design wavelength of 1.55 µm. The vertical stack of the considered CRIGF (see Fig. 1(a)) is a 300-nm-thick waveguiding layer of lithium niobate ($n_L = 2.1362$ at 1.55 µm) on a glass substrate ($n_s = 1.4440$ at 1.55 µm), covered with a fully-etched 50 nm thick lamellar grating made of Si_3N_4 ($n_G = 1.9963$ at 1.55 µm). These values were chosen as 300 nm is the thinnest commercially available lithium niobate on insulator layer, and the grating thickness was adjusted to present a good compromise between the DBR mirror parameters (reflectivity and bandwidth) and GC coupling strength.

As the real part of the guided mode effective index is approximately equal to 1.7725, we fix the groove period d_{GC} to $1.55/1.7725 \approx 0.87446$ µm to achieve a 1.55 µm resonance. The two grooves inside each period (Fig. 2) have the same width $c_{GC}/2 = 0.225$ µm, and the bump widths a_1 and a_2 depend on δ. At a fixed groove depth, the strength of the excitation of the guided mode is proportional the square of the perturbation δ [5]. This strength can be expressed either as the imaginary part n''_{eff} of the effective index of the mode, or as the imaginary part $\lambda^{p''}$ of the wavelength pole λ^p of the system:

$$\lambda^p = \lambda^{p'} + i\lambda^{p''}. \qquad (2)$$

The Q-factor of the infinite grating is then simply given by the ratio between the real and imaginary parts of the pole:

$$Q_{inf} = \frac{\lambda^{p'}}{2\lambda^{p''}} \sim \frac{1}{\delta^2}. \qquad (3)$$

The factor 2 in the denominator stems from the fact that the Q-factor is related to the field mode intensity, while the pole and zero originate from the modal amplitude excitation. Table 1 gives the values of the pole imaginary part and the corresponding Q-factor calculated with FMM for a set of δ values. These results are consistent with Eq. (3).

As already mentioned, in the case of an infinite grating illuminated by a plane wave, the grating equation implies that spectral width and angular tolerances are tightly coupled. A higher Q-factor (and thus a spectrally narrower resonance) implies tighter angular tolerances and larger excitation beams. In particular, GMRFs with $Q \sim 10^6$ typically exhibit sub-0.1° angular acceptance angle and need to be probed with millimetre-waist Gaussian beams.

Table 1. Properties of the infinite-size GC as a function of δ.

δ (nm)	20	10	5	2.5	1.25	0.625	0.3125
$\lambda^{p''}$ ($\times 10^{-6}$)	70.2	17.7	4.42	1.1	0.276	0.069	0.0173
Q_{inf} ($\times 10^6$)	0.011	0.044	0.175	0.704	2.81	11.2	44.8

When placed in a Bragg-grating mirror cavity, the dispersion curve is flattened [22] (see Appendix), so that a device having 21 grooves for the GC (i.e. a GC length of 18 µm), can be used with focused incident beam having a waist $w = 9$ µm, while maintaining a resonant reflection maximum greater than 80%. The flattening of the dispersion curve is easily explained by the fact that the resonant wavelength is determined by the external (Bragg) resonator and does not depend on the incident angle. The latter only determines the efficiency of the mode excitation by the GC.

The period of the DBR d_{DBR} is half the GC period d_{GC}, and determined by the equation:

$$d_{BG} = \lambda/(2n'_{eff}). \tag{4}$$

where n'_{eff} is the real part of the mode propagation constant. To maximize the DBR reflectivity its filling factor is usually taken to be equal to 50% ($c_{DBR} = 0.5d_{DBR}$). However, with h = 50 nm, the DBR reflectivity spectral region only extends over 20 nm, and effective index mismatch between the GC and DBR moves the GC resonance wavelength out of the DBR reflectivity stopband. In order to compensate for this mismatch and bring back the GC wavelength within the stop band we set $c_{DBR} = 160$ nm, equal to 0.456 times d_{DBR}. The spectral position of the reflection maximum can then be fine-tuned by varying the distance between the GC and DBR regions, which we denote by Δ (see Fig. 1(a)).

In a CRIGF, as the GC is inside a cavity, its Q-factor, Q_{GC}, increases because the mode extends inside the DBR mirrors over an effective length, while the in/outcoupling radiation losses only occur inside the GC region:

$$Q_{GC} = Q_{inf} \frac{L}{L_{GC}} = \frac{\lambda^{p'}}{2\lambda^{p''}} \frac{L}{L_{GC}}, \tag{5}$$

where

$$L = L_{GC} + 2L_{eff} \tag{6}$$

and L_{eff} is the effective length of the penetration of the mode energy inside the mirrors [23]:

$$L_{eff} = \frac{\tanh(\gamma_{DBR}L_{DBR})}{2\gamma_{DBR}}. \tag{7}$$

γ_{DBR} and L_{DBR} respectively being the rejection strength and physical length of the DBRs. In our case γ_{DBR} is ~0.0454 μm^{-1}, and L_{eff} is ~11 μm. The overall Q-factor of the system, Q_{CRIGF}, is determined by the in/outcoupling radiation losses of the GC and the intrinsic Q-factor of the uncoupled (δ (or η) tending to 0) FP cavity, Q_{FP}:

$$\frac{1}{Q_{CRIGF}} = \frac{1}{Q_{GC}} + \frac{1}{Q_{FP}}. \tag{8}$$

Neglecting all other types of losses, Q_{FP} is limited by the leakage through the DBR mirrors, Q_{DBR}, which can be expressed as:

$$Q_{DBR} = \frac{2\pi n_{eff}L}{\lambda T_{DBR}}, \tag{9}$$

where T_{DBR} is the transmission coefficient of the DBR and is given by the relation:

$$T_{DBR} = 1 - R_{DBR} = 1 - \tanh(\gamma_{DBR}L_{DBR}). \tag{10}$$

Given the rejection strength of the DBR, we consider 400-groove DBRs (with total length $L_{DBR} = 400 \, d_{DBR}$) as these mirrors reflect more than $R_{DBR} = \tanh(\gamma_{DBR}L_{DBR}) = (1 - 2.10^{-7})$ parts of the mode amplitude [24] and lead to a Q_{DBR} of 1.45×10^9.

However, FMM calculations of Q_{CRIGF} systematically show asymptotic intrinsic Q-factors (achieved for δ (or η)→0) that are much lower than the above-mentioned value of Q_{DBR}, even with Q_{GC} tending to infinity. Therefore, an additional loss must be present in the system and that is not included in this simple analysis.

In the real world, there could be several important losses, for example; material absorption, surface roughness scatter, mode spatial spreading between the DBR mirrors, and grating

inhomogeneities. However, all these technologically related losses are eliminated in the theoretical-numerical model used here. The loss that remains in our calculations is the scatter S_{tr} due to the transition losses at the junctions between different gratings. Taking this into account and assuming that the losses due to the DBR leakage are much smaller than scattering losses, Q_{FP} can be written in the form:

$$Q_{FP} \approx \frac{2\pi n_{eff} L}{\lambda S_{tr}}. \tag{11}$$

where S_{tr} is the scattering loss per cavity round trip.

Considering our design K_0, the junction length Δ (Fig. 1(a)) is found to be of the order of 0.82 μm, almost twice the wavelength of the standing wave of the waveguide mode inside the resonator, and has a real part of the mode propagation constant different from the ones inside the GC and DBR regions (which are both the same by design). This difference in mode propagation causes scattering at the interfaces between these zones. As proposed in [14], it is possible to significantly reduce S_{tr} by dividing the junction in two segments with a single groove whose width is optimized numerically. This configuration is denoted as K_1 (Fig. 1(b)).

Another source of scattering comes from the differences in the imaginary parts of the propagation constant of the mode in the different regions of the device. The imaginary part of the mode propagation constant in the DBR is equal to $\gamma_{DBR} \approx 0.0454$ μm^{-1}, whereas inside the GC it can be as small as $\gamma_{GC} \approx 10^{-8}$ μm^{-1}. To limit these losses, we chose to use the apodizing technique, which is well known to allow modal adaptation between different regions. This consists of gradual change of geometrical parameters inside the junction region between the DBRs and the GC. In this configuration, K_{apo}, the junction is separated into two regions J_{apoA} and J_{apoB} (see Fig. 1(c)). Region J_{apoA} gradually reduces the value of δ towards that of the DBR configuration ($\delta = 0$). However, this section does not have the same filling factor as the cavity DBR, which is equal to 0.465. Region J_{apoB}, set between region J_{apoA} and the DBR, gradually adapts the filling factor from 0.5 to 0.456.

In practice, Region J_{apoA}, close to the GC, has 9 GC grooves and a length of 8 μm with a linearly decreasing value of δ down to zero, keeping the same groove width, $c_{GC}/2 = 225$ nm. Region J_{apoB} has 9 grooves with $\delta = $ gra0 and a groove width that gradually varies from 225 to 160 nm. Region J_{apoA} also serves as a part of GC in- and out-coupling, thus the length of the GC is reduced from 21 to 11 grooves to maintain an optimal coupling with an incident beam of 9 μm waist. The resulting total length of the device is slightly increased from 324 to 342 μm. Note that for the two smallest δ values ($\delta = 0.625$ and 0.3125 μm) region J_{apoA} is not used as it does not improve the Q-factor.

3.   Q-factor and coupling regimes

Our goal is to study the transition between a situation where the coupling is dominated by the GC and a case where it is dominated by the cavity scattering. Therefore, we studied the three designs shown in Fig. 1 with varying values of δ.

Figure 3 shows in solid black line the in/out coupling Q-factor, Q_{GC}, as calculated by Eq. (5), as a function of η (as defined by Eq. (1) in section 2) and δ on the top axis. Each solid color line corresponds to the intrinsic Q-factor of the uncoupled cavity (red for configuration K_0, blue for K_1 and magenta for K_{apo}) while each solid color line with symbols represents the CRIGF Q-factor calculated with FMM (red for configuration K_0, blue for K_1 and magenta for K_{apo}).

As expected, irrespective of the junction design, the behavior of Q_{CRIGF} asymptotically matches Q_{GC} for high coupling (high η values) cases. Q_{GC} follows a δ^{-2} dependence as highlighted by Eq. (3) and (5). Having considered a CRIGF with DBRs exhibiting a 0.0454/μm rejection strength and with a GC whose length L_{GC} was taken to be 18 μm for optimal excitation by a 9-μm-waist Gaussian beam, the plotted Q_{GC} values are enhanced by a factor $(L_{GC} + 2L_{eff})/L_{GC} = 40/18$ with respect to the values provided in Table 1.
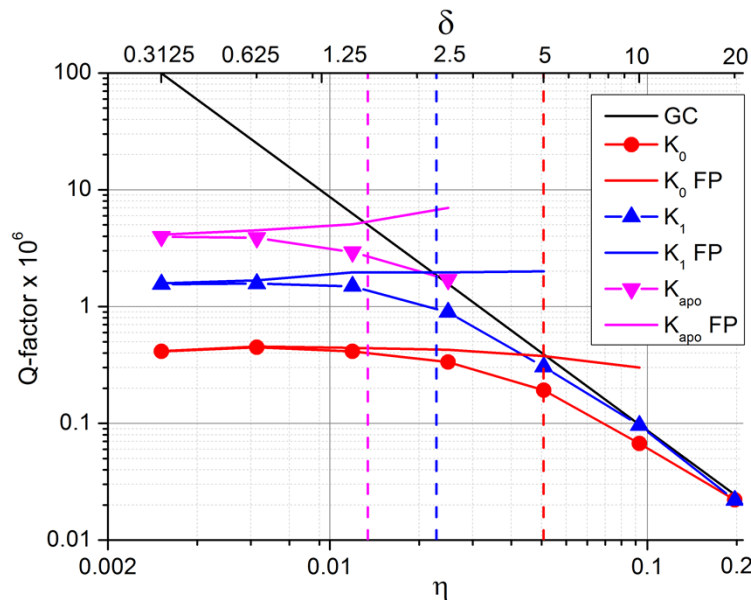
Fig. 3. Q-factor (in million) as a function of η: black line Q_{GC} (Eq. (4)), red circles and red line, Q_{CRIGF} and Q_{FP} for the case K_0 without supplementary groove; blue triangles and blue line, Q_{CRIGF} and Q_{FP} for the case K_1 with a supplementary groove in the junction of GC and DBR; magenta inverted triangles and magenta line, Q_{CRIGF} and Q_{FP} for the K_{apo} case. The top scale gives the values of δ in nm.

When decreasing the grating strength (η), the deviation of Q_{CRIGF} from Q_{GC} gradually increases, Q_{CRIGF} reaching a saturation limit for small η which corresponds to the intrinsic Q-factor, Q_{FP} is determined according to Eq. (8). Furthermore, this intrinsic Q-factor is seen to be influenced by the DBR-to-GC junction design as the saturation value increases when the junction is changed from K_0 to K_1 and from K_1 to K_{apo}. This observation highlights the fact that the junction design can be a performance-limiting factor in the CRIGF response, that the proposed approach to reduce the scattering losses is indeed effective, and that the maximum achievable Q-factors can be raised to values in excess of 10^6.

By analogy with ring resonators [25], the large η (respectively small η) region in Fig. 3 is ascribed as the over-coupling (respectively under-coupling) region. Indeed, large profile perturbations lead to values of Q_{GC} much smaller than Q_{FP} and thereby the Q_{CRIGF} is limited by Q_{GC}. With smaller profile perturbation parameter η, Q_{GC} grows and, consequently, Q_{CRIGF} also increases. Q_{FP} is not affected by that change and stays almost constant and independent of η. Approaching the so-called critical coupling [20,25] defined by $Q_{GC} = Q_{FP}$, Q_{CRIGF} grows less rapidly and becomes equal to $Q_{GC}/2$ at the critical point. In the case of K_0 this happens for $\eta = 0.047$, for K_1, at approximatively $\eta = 0.024$, and with apodization K_{apo}, for $\eta = 0.014$. To the left of the latter critical point, Q_{CRIGF} becomes limited by Q_{FP} ($Q_{FP} \ll Q_{GC}$), and the operation enters the under-coupling regime.

Yariv [20] has pointed out that critical coupling must lead to an enormous enhancement of the modal field inside the resonator, no matter the excitation process. Indeed, Fig. 4(a) shows the values of the electric field maximum E_{max} (calculated at the center of the lower interface of core layer of the CRIGF (point (0,0) in Fig. 1(a), and normalized with respect to the incident field), for the three different CRIGF configurations. As expected from Yariv's work, the maxima of E_{max} appear quite close to the positions of the critical coupling.
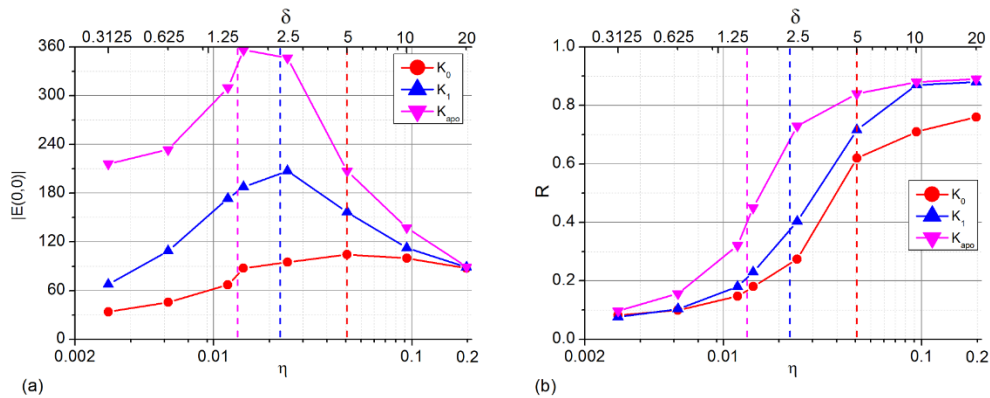
Fig. 4. Dependence of (a) the amplitude of the electric field in the middle of the structure (x = z = 0 in Fig. 1(a)) and of (b) the reflectivity maximum as a function of the perturbation parameter for the three types of junctions. δ is given in nm.

Figure 4(b) presents the reflectivity maxima as a function of the perturbation parameter. Contrary to ring resonators, where the minimum in transmission reaches 0 at the critical coupling, here we observe quite a different behavior. In the over-coupling zone, the reflectivity is maximal (i.e. the transmission is minimal), decreases rapidly at critical coupling, and quickly saturates at much lower value in the under-coupling region. The explanation is quite simple. In the over-coupled regime, the predominant losses come from the radiation by the GC in the cladding and the substrate, which, in fact is the grating contribution to the resonant Fano-type anomaly in reflection. This resonant contribution is responsible for the 100% maximum of R for an infinite grating with plane wave illumination. On the other hand, the scattering losses in Q_{FP} at the junctions between different regions have non-specular character, and do not contribute to the resonance in reflection. Moreover, they grow proportionally to the field intensity, which is maximal at critical coupling. This behavior is fairly general and is found to be similar to the result described in [26], except that the bound states in [26] are symmetry-protected

Figures 3 and 4(a) confirm the interest of mode matching the different regions. Even the simplest introduction of an additional groove at the junctions leads to an almost 3-time increase of the Q-factor for δ = 2.5 nm, and similar increase in the electric field amplitude. Adding an apodization region helps gaining another 2.1 times increase of the Q-factor. Almost half of it is due to the increase in the effective resonator length while the remainder comes from the apodizing effect. At smaller η the increase can reach more than 10 time.

4. Conclusions

The analysis of the response of resonators in terms of coupling regimes has been extended to Cavity-Resonant Integrated-Grating Filters. In particular, it has been shown that the device behavior can be continuously adjusted by varying the profile of the (bi-atom) internal grating coupler from the over-coupling regime dominated by this grating in/outcoupling radiative loss to the under-coupling regime limited by the intrinsic resonator scattering losses.

A first practical conclusion of this study is that, should the device be used as a narrow-band reflection filter, the operating regime should be restricted to the over-coupling domain since in this case, the resonant peak reflectivity (respectively transmission) is maximized (respectively minimized). Additionally, should the CRIGF serve as local field amplifier, as for non-linear operation for instance, the best performance will be obtained, as with other resonators, close to the critical coupling condition. However, CRIGFs do not exhibit an obvious signature when operating

at critical coupling, contrary to ring resonators. This will lead to an additional experimental difficulty in the optimization of the device performance. However, the difficulty is compensated by the rather large tolerances in terms of η values required to achieve critical coupling.

Last but not least, we have established that, using an appropriate mode matching technique, the achievable Q-factors can in theory reach several millions, values close to the best Q-factors achieved in other waveguide resonators, namely whispering gallery mode resonators [27–29] and photonic crystal cavities [30].

Concerning other potential losses, preliminary calculations shows that Q-factors larger than 10^5 can be achieved with our designs provided that the imaginary part of the optical index of the layers is lower than 10^{-5}, corresponding to 3.5dB/cm losses, which strengthen the potential of this approach.

5. Appendix: Spatial Fourier presentation of the modal field

An infinitely long plane waveguide supports guided modes having a Dirac-function spectral and angular response:

$$\exp(i\alpha^p x), \tag{12}$$

where $\alpha^p = k_0 n_{eff}$ is the mode propagation constant. When put in a cavity with a length L, the angular width is enlarged to $4\pi/L$:

$$\exp(i\alpha^p x) \rightarrow L \frac{\sin(\alpha - \alpha^p)\frac{L}{2}}{(\alpha - \alpha^p)\frac{L}{2}}, \tag{13}$$

In the CRIGF device, as the incident field has a Gaussian form (both in the direct and the inverse space), the modal field Fourier distribution is a convolution between the sample function (Eq. 13) and the Gaussian beam. As the waist of the latter is matched to the length of the GC region, they have similar width in the inverse space. For example, if the waist is 5 μm and the optimal effective length is about 40 μm, the corresponding width in the inverse space are of the order of 0.3 μm^{-1}, independent of the value of δ.

Disclosures. Authors declare no conflict of interest.

Data availability. Data underlying the results presented in this paper are not publicly available at this time but may be obtained from the authors upon reasonable request.

References

1. K. Knop, "Diffraction gratings for color filtering in the zero diffracted order," Appl.Opt. **17**(22), 3598–3603 (1978).
2. L. Mashev and E. Popov, "Zero Order Anomaly of Dielectric Coated Grating," Opt. Commun. **55**(6), 377–380 (1985).
3. U. Fano, "The theory of anomalous diffraction gratings and of quasi-stationary waves on metallic surfaces (Sommerfeld's waves)," J. Opt. Soc. Am. **31**(3), 213–222 (1941).
4. A. Hessel and A. A. Oliner, "A new theory of Wood's anomalies on optical gratings," Appl. Opt. **4**(10), 1275–1297 (1965).
5. E. Popov, L. Mashev, and D. Maystre, "Theoretical Study of the Anomalies of Coated Dielectric Gratings," Opt. Acta **33**(5), 607–619 (1986).
6. J. M. Bendickson, E. N. Glytsis, T. K. Gaylord, and D. L. Brundrett, "Guided-mode resonant subwavelength gratings: effects of finite beams and finite gratings," J. Opt. Soc. Am. A **18**(8), 1912–1928 (2001).
7. F. Lemarchand, A. Sentenac, E. Cambril, and H. Giovannini, "Study of the resonant behaviour of waveguide gratings: increasing the angular tolerance of guided-mode filters," J. Opt. A: Pure Appl. Opt. **1**(4), 545–551 (1999).
8. S. Ura, S. Murata, Y. Awatsuji, and K. Kintaka, "Design of resonance grating coupler," Opt. Express **16**(16), 12207–12213 (2008).
9. Y. Zhou, M. Moewe, J. Kern, M. C. Y. Huang, and C. J. Chang-Hasnain, "Surface-normal emission of a high-Q resonator using a subwavelength high-contrast grating," Opt. Express **16**(22), 17282–17287 (2008).
10. S. Ura, J. Inoue, K. Kintaka, and Y. Awatsuji, "Proposal of small-aperture guided-mode resonance filter," in *International Conference on Transparent Optical Networks* (IEEE, 2011), paper Th.A4.4.

11. X. Buet, E. Daran, D. Belharet, F. Lozes-Dupuy, A. Monmayrant, and O. Gauthier-Lafaye, "High angular tolerance and reflectivity with narrow bandwidth cavity-resonator-integrated guided-mode resonance filter," Opt. Express **20**(8), 9322–9327 (2012).

12. X. Buet, A. Guelmani, A. Monmayrant, S. Calvez, F. Lozes-Dupuy, and O. Gauthier-Lafaye, "Robust and simplified cat's-eye external-cavity lasers using cavity resonant integrated grating filters," in *International Conference on Transparent Optical Networks* (IEEE, 2013), paper We.B2.2.

13. J. Inoue, T. Ogura, T. Kondo, K. Kintaka, K. Nishio, Y. Awatsuji, and S. Ura, "Reflection characteristics of guided-mode resonance filter combined with bottom mirror," Opt. Lett. **39**(7), 1893–1896 (2014).

14. F. Renaud, A. Monmayrant, S. Calvez, O. Gauthier-Lafaye, A.-L. Fehrembach, and E. Popov, "Second-harmonic-generation enhancement in cavity resonator integrated grating filters," Opt. Lett **44**(21), 5198–5201 (2019).

15. S. Yuan, Y. Wu, Z. Dang, C. Zeng, X. Qi, G. Guo, X. Ren, and J. Xia, "Strongly Enhanced Second Harmonic Generation in a Thin Film Lithium Niobate Heterostructure Cavity," Phys. Rev. Lett. **127**(15), 153901 (2021).

16. A. Fehrembach, F. Renaud, E. Popov, H. Tortel, A. Monmayrant, O. Gauthier-Lafaye, and S. Calvez, "Dark mode-in-the-box for enhanced second-harmonic generation in corrugated waveguides," Opt. Express **29**(25), 40981–40992 (2021).

17. S. Pelloquin, S. Augé, K. Sharshavina, J.-B. Doucet, A. Héliot, H. Camon, A. Monmayrant, and O. Gauthier-Lafaye, "Soft mold NanoImprint Lithography: a versatile tool for sub-wavelength grating applications," Microsyst Technol., 1–8 (2018).

18. L. Li, "New formulation of the Fourier modal method for crossed surface-relief gratings," J. Opt. Soc. Am. A **14**(10), 2758–2767 (1997).

19. P. Chaumet, G. Demésy, O. Gauthier-Lafaye, A. Sentenac, E. Popov, and A.-L. Fehrembach, "Electromagnetic modeling of large subwavelength-patterned highly resonant structures," Opt. Lett. **41**(10), 2358–2361 (2016).

20. A. Yariv, "Universal relations for coupling of optical power between microresonators and dielectric waveguides," Electron. Lett. **36**(4), 321–322 (2000).

21. F. Lemarchand, A. Sentenac, and H. Giovannini, "Increasing the angular tolerance of resonant grating filters with doubly periodic structures," Opt. Lett. **23**(15), 1149–1151 (1998).

22. N. Rassem, A.-L. Fehrembach, and E. Popov, "Waveguide mode in the box with an extraordinary flat dispersion curve," J. Opt. Soc. Am. A **32**(3), 420–430 (2015).

23. D. Babic and S. Corzine, "Analytic expression for the reflection delay, penetration depth, and absorptance of quarter-wave dielectric mirrors," IEEE J. QE **28**(2), 514–524 (1992).

24. A. Yariv, "Coupled-mode theory for guided-wave optics," IEEE J. QE **9**(9), 919–933 (1973).

25. Y. Dumeige, S. Trebaol, L. Ghis, T. K. N. Nguyên, H. Tavernier, and P. Féron, "Determination of coupling regime of high-Q resonators and optical gain of highly selective amplifiers," J. Opt. Soc. Am. B **25**(12), 2073–2080 (2008).

26. K. Koshelev, Y. Tang, K. Li, D.-Y. Choi, G. Li, and Y. Kivshar, "Nonlinear Metasurfaces Governed by Bound States in the Continuum," ACS Photonics **6**(7), 1639–1644 (2019).

27. J. Hu, N. Carlie, N. Feng, L. Petit, A. Agarwal, K. Richardson, and L. Kimerling, "Planar waveguide-coupled, high-index-contrast, high-Q resonators in chalcogenide glass for sensing," Opt. Lett. **33**(21), 2500–2502 (2008).

28. D.-P. Cai, J.-H. Lu, C.-C. Chen, C.-C. Lee, C.-E. Lin, and T.-J. Yen, "High Q-factor microring resonator wrapped by the curved waveguide," Sci Rep **5**(1), 10078 (2015).

29. Y.-X. Yin, X.-P. Zhang, X.-J. Yin, Y. Li, X.-R. Xu, J.-M. An, Y.-D. Wu, X.-P. Liu, and D.-M. Zhang, "High-Q-Factor Tunable Silica-Based Microring Resonators," Photonics **8**(7), 256 (2021).

30. Y. Akahane, T. Asano, B.-S. Song, and S. Noda, "High-Q photonic nanocavity in a two-dimensional photonic crystal," Nature **425**(6961), 944–947 (2003).